2014 CMBEC37 Conference
Vancouver, BC
May 21 – 23, 2014

# Multimode imaging applied toward diagnosis of skin cancer (SkinSpect)

*Fartash Vasefi [a], Nicholas MacKinnon [a], Daniel L. Farkas [a, b],*
*[a] Spectral Molecular Imaging Inc., Beverly Hills, CA, USA*
*[b] Dept. of Biomedical Engineering, University of Southern California, Los Angeles, CA, USA*

## ABSTRACT

We introduce the research prototype of SkinSpect – a multimode dermoscope combining fluorescence, polarization and hyperspectral imaging. The multimode dermoscope combines polarization and hyperspectral imaging with a computationally rapid analytical model. This approach employs specific spectral ranges in visible and near infrared wavelengths for mapping the distribution of specific skin bio-molecules. This corrects for the melanin-hemoglobin misestimation common to other systems, without resorting to complex and computationally intensive tissue optical models that are prone to inaccuracies due to over-modeling. In the example shown, skin with a melanocytic nevus was imaged, after which the system determined relative melanin and hemoglobin concentrations as well as skin surface "fabric pattern" and fluorescence anisotropy maps.

## INTRODUCTION

The present common standard in melanoma patient care is a dermatologist's visual examination [1] - [5], in which the practitioner looks for abnormalities in mole shape, size and color. Around 2 million biopsies are performed annually to detect melanoma, and the vast majority of these (over 80%) are benign [6]. An approach to enhance evaluation can include a dermoscope with (low power) magnification and/or specific illumination [7][8]. Many dermatologists are also adopting new dermoscopes providing different wavelengths of light, higher magnification, or more advanced computer algorithms to provide enhanced diagnostic information.

Recently, more complex imaging/sensing systems that quantify anatomical and physiological information about skin constituents such as SIAscope IV [9] have been developed. Instrumentation employing intracutaneous analysis with SIAscopy is designed to provide mapping of skin chromophores (melanin, hemoglobin, and collagen). It was reported to have high sensitivity of 96.2 % but the specificity was low at 56.8% [9]. A recent independent study published in 2013 [10] concluded that: (i) SIAscopy-based results have low diagnostic accuracy for melanoma, (ii) single SIAscopic features do not provide reliable diagnostic information relating to the lesions' internal structure on histopathology examination and (iii) SIAscopy cannot be used as a guide for localizing the maximum lesion thickness (for histopathological examination).

Systems such as the MelaFind (using more wavelengths compared to SIAscopy) and Verisante Aura (using Raman spectra), employ statistical classifiers, sometimes called "blackbox" methods, to analyze optical measurements [11][12]. While these systems provide high sensitivity, they fail to achieve a desirable level of specificity. As studies with these devices progress from smaller to larger populations, they have shown significant reductions in specificity. Telling examples are the specificity reduction for MelaFind; specificity from 85% [13] to 9.9% [14]. For Verisante Aura specificity dropped from 78% [15] to 15% [12]. As reflected in these studies, the statistical classification approach shows barriers to success, when seemingly promising clinical devices fail to perform in larger studies. Our SkinSpect system works with tissue model-based algorithms and unlike those employing statistical classifiers does not require larger population trials to generate learning and testing sets.

## MATERIALS AND METHODS

The SkinSpect imaging system combines fluorescence, polarization control and hyperspectral imaging technologies. Each scan generates an image of skin 11 mm × 16 mm in size. The data acquisition is a sequential imaging of the object at the following illumination wavelengths: blue, green, red to form an RGB color image, 385 nm (fluorescence excitation), followed by sequential band illumination of 33 wavelength from 480 nm to 900 nm. The sequential data acquisition allows us to optimize the illumination and camera exposure time for each image to maintain the required signal to noise. As seen in Figure 1, we developed one SkinSpect research prototype unit with customized image acquisition and a GUI software package that enables new levels of detail in the measurement of skin lesions. The system consists of a console that houses a light source; computerized system controller; operator input and image capture software; communication interfaces and a handpiece probe that can easily be moved as needed to survey the skin of a patient. The console module houses the (spectral) illumination source, a UNIX operating computer which controls the handpiece illumination, data acquisition, image processing archiving and data transmission, and a touch-screen Windows computer to facilitate patient record data management and visual interfaces

The handpiece in the research prototype (Figure 1) device employed two cameras, two polarizers, and a pellicle beam-splitter that enables the capture of images in both parallel and cross polarization states (more details in [16][17]) . These two states are required to get the advantages of polarization-based imaging discussed above, such the removal of specular reflection [17], enhancement of signals from the lower layers, and discerning the depth of a suspected melanoma. We evaluated this research prototype unit and identified several opportunities for improvement. These are: (1) illumination intensity and scanning acquisition speed, (2) reduction of spectral and other effects from the pellicle beamsplitter, (3) ease of use and better lesion targeting with a handpiece-mounted viewfinder, and (4) enhancements to image registration between the cameras.

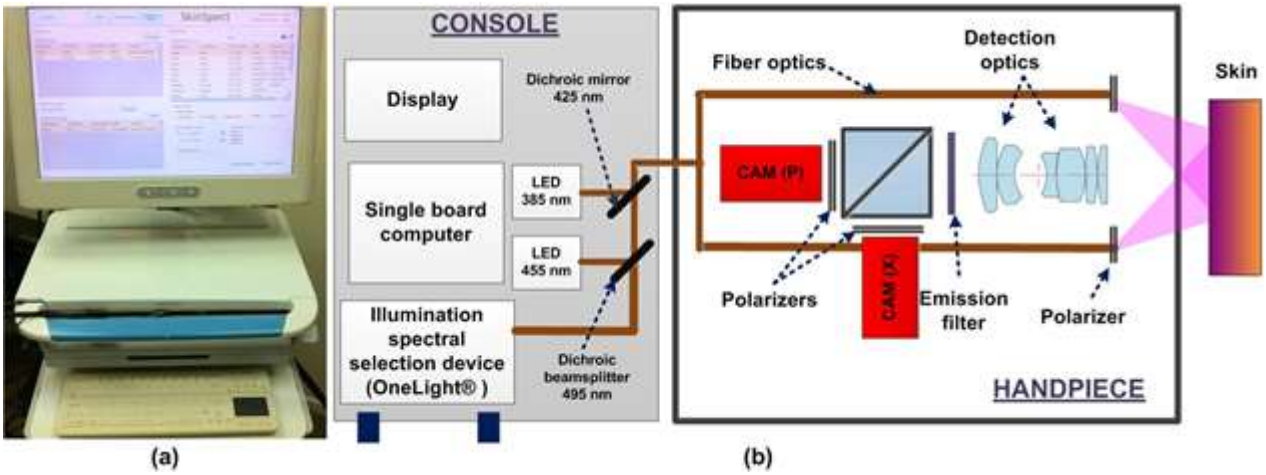


Figure 1: SkinSpect research prototype: (a) system console (b) system diagram

## RESULTS AND DISCUSSION

Optical design specifications of our prototype instrument are presented. Spectral programming of the light source (OneLight®) is optimized to improve the accuracy of skin chromophore quantitation. Polarized attenuation spectra were computed from parallel and cross-polarized reflectance datacubes and then input into a wavelength-dependent linear model to extract the relative

contributions of chromophores according to Beer-Lambert. The total hemoglobin concentration, and concentrations of melanin were derived and compared for normal and pigmented nevus regions.

Skin "fabric pattern"

A study published in 2012 [18] shows that skin cancer usually disrupts the skin surface "fabric pattern" which allows the margins to be delineated more accurately than via regular dermoscopy, using polarization imaging revealing skin surface structure by removing the obscuring diffuse reflectance.

Based on such observations, and unlike other commercial devices, the SkinSpect provides access to this useful information about skin surface topography by extracting the polarization maps of skin as shown in eq. (1) and (2):

$$Z_{\parallel}(x,y,\lambda) = \frac{R_{\parallel_{skin}}(x,y,\lambda)}{R_{\parallel_{spectralon}}(x,y,\lambda)}, \quad \text{and} \tag{1}$$

$$Z_{\perp}(x,y,\lambda) = \frac{R_{\perp_{skin}}(x,y,\lambda)}{R_{\perp_{spectralon}}(x,y,\lambda)}$$

where the calibrated image-cubes in both parallel ($Z_{\parallel}$) and perpendicular ($Z_{\perp}$) polarization states are computed using the equation (1). $R_{\parallel skin}$ and $R_{\perp skin}$ are the reflectance measurements of skin hyperspectral images by parallel and cross polarized cameras. $R_{\parallel spectralon}$ and $R_{\perp spectralon}$ are the reflectance measurements of Spectralon hyperspectral images by the same parallel and cross-polarized cameras.

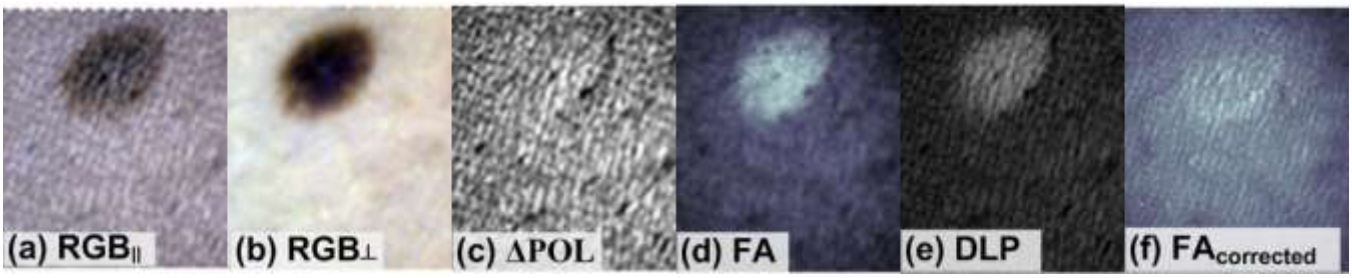


Figure 2. SkinSpect image output: RGB color image (a) in parallel polarization, (b) in prependiculat polarization, (c) skin "fabric pattern" map at 455 nm, (d) fluorescence anisotropy map, (e) degree of linear polarization map at 455 nm, (f) melanin corrected fluorescence anisotropy map

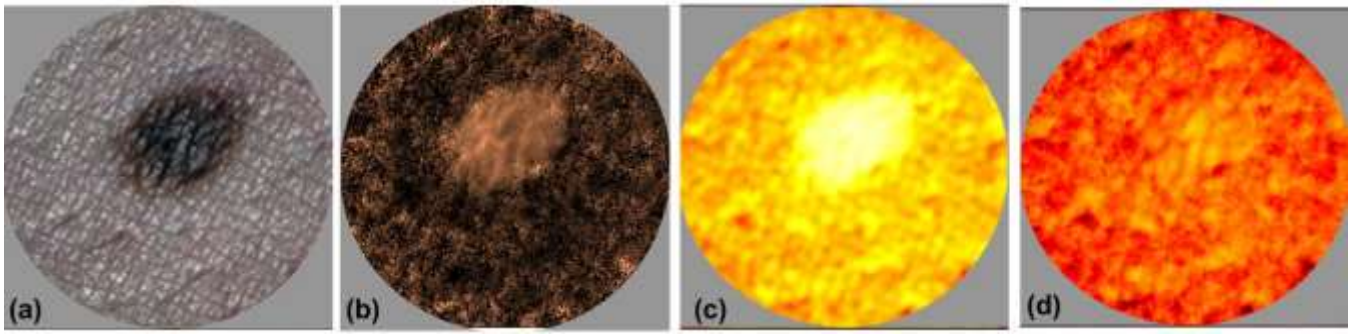


Figure 3. Skin with melanocytic nevus (a) RGB color image, (b) estimated deep melanin concentration map, total hemoglobin concentration map (c) before melanin correction, (d) after melanin correction

The tissue surface profile can be extracted using ΔPOL (x,y,λ) as below:

$$\Delta POL(x,y,\lambda) = Z_{\parallel}(x,y,\lambda) - Z_{\perp}(x,y,\lambda) \tag{2}$$

patterns of the skin with melanocytic nevus (at 455 nm) compared with RGB color images in parallel (Figure 2a) and perpendicular (Figure 2b) polarization modes.

Fluorescence Anisotropy

Each spatial coordinate in SkinSpect data contains full normalized reflectance spectra (Figure 5a and e) in both parallel and cross polarization and derived data such as degree of linear polarization as described below:

$$DLP(x,y,\lambda) = \frac{Z_{\parallel}(x,y,\lambda) - Z_{\perp}(x,y,\lambda)}{Z_{\parallel}(x,y,\lambda) + Z_{\perp}(x,y,\lambda)} \quad (3)$$

A DLP spatial map at 455 nm is shown in Figure5c and g for skin with melanocytic nevus and vitiligo conditions. The layered structure of the skin and the biochemical composition generates distinct fluorescence and polarization properties for each layer of the skin. For instance, major fluorophores in the epidermis are NADH, NADPH, FAD, keratin, and some amino acids, while in the dermis, collagen and elastin are the major fluorophores [19]. In the SkinSpect research prototype 385 nm LED excitation provides fluorescence images at parallel and cross polarization. At this excitation wavelength, fluorescence originates from FAD, and collagen or elastin cross-links [19][20][21].

SkinSpect provides polarized excitation and illumination and captures polarized fluorescence emission. The degree to which the fluorescence emission is polarized can be described quantitatively by the Fluorescence Anisotropy factor [19][22] (FA):

$$FA(x,y) = \frac{I_{F\parallel}(x,y) - I_{F\perp}(x,y)}{I_{F\parallel}(x,y) + 2I_{F\perp}(x,y)} \quad (4)$$

The calculation of fluorescence anisotropy appears to cancel out the common absorption effect of superficial melanin, further facilitating the discrimination of pigmented skin lesions. Many researchers have shown dependence of FA on dermal thickness (see e.g. [19][23]).

Skin with higher melanin (e.g. mole areas) appears bright in the FA image compared to surrounding normal skin (Figure 2d). Since SkinSpect allows determination of both FA and DLP (Figure 2e) maps and since fluorescence photons experience the same scattering and absorption events as diffuse reflectance photons (in the emission wavelength range) when backscattering from a tissue [24], FA and DLP can be combined to correct the melanin attenuation artifact in the FA image (Figure 2f) [19][23]. Furthermore, polarized fluorescence can detect differences in the physical and chemical properties of the targeted fluorophores and their microenvironment [24], providing an additional means for enhancing the contrast needed for melanoma detection using autofluorescence methods [25].

SkinSpect correction of hemoglobin misestimation

Figure 3 shows the derived chromophore maps of the skin with a melanocytic nevus. The skin melanin maps (see Figure 3b) were calculated from the slope of polarization attenuation spectra between 600 nm - 700 nm, $A_{POL}$ as described below:

$$A_{POL} = log\left(\frac{Z_{\parallel} - Z_{\perp}}{Z_{\parallel}}\right) \quad (5)$$

where ($Z_{\parallel}$) and ($Z_{\perp}$) are the calibrated image cubes in both parallel polarization states. Figure 6d shows how a high melanin concentration is conducive to mis-estimation of hemoglobin concentrations. We applied our deep melanin estimation method described above to correct this hemoglobin mis-estimation. Figure 3c shows how this approach corrects the hemoglobin over-estimation in the nevus. The melanin ($A_{POL-Mel\,corrected}$) corrected polarized attenuation spectrum was employed for hemoglobin estimation using a two-chromophore (oHb and Hb) model and curve-fitting algorithms with the extinction coefficients of oHb and Hb as primary vectors in the 500 nm - 577 nm spectral range. More detail about the algorithm is presented in [17]. By comparing Figure 3c and Figure 3d, it is clear that without the melanin correction step, the skin area with a strong melanin contribution leads to hemoglobin overestimation while melanin correction causes the biologically implausible melanin-related hemoglobin artifact to be nearly eliminated.

## CONCLUSION

We have used SkinSpect's polarization-sensitive hyperspectral imaging system as a new, advanced, clinical dermoscope for in vivo skin analysis. The resulting data suggest that the system is useful for extracting and quantifying relative chromophore concentrations in skin

tissues, especially highly pigmented lesions, in a topologically resolved manner.

## ACKNOWLEDGEMENTS

We thank our colleagues and collaborators, and particularly Drs. A. Durkin and R. Saager (UC Irvine) and Drs. M. Rajadhyaksha, A. Marghoob and A. Halpern (Memorial Sloan Kettering Cancer Center) for very helpful discussions and suggestions pertaining to this work. Dr. Farkas and Spectral Molecular Imaging, Inc. acknowledge the US Department of Health and Human Services for support under the Qualifying Therapeutic Discovery Program of the Patent Protection and Affordable Care Act of 2010.

## REFERENCES

[1] Benelli, C., Roscetti, E., Dal Pozzo, V., Gasparini, G., and Cavicchini, S., "The dermoscopic versus the clinical diagnosis of melanoma," Eur J Dermatol, 9(6), 470-476 (1999).

[2] Du Vivier, A.W., Williams, H.C., Brett, J.V., Higgins, E.M., "How do malignant melanomas present and does this correlate with the seven-point checklist? ," Clin Exp Dermatol 16(5), 344–347 (1991).

[3] Higgins E. M., Hall, P., Todd, P., Murthi, R., Du Vivier, A.W., "The application of the seven-point check-list in the assessment of benign pigmented lesions, " Clin Exp Dermatol 17(5), 313-315 (1992).

[4] McGovern, T.W., Litaker, M.S., "Clinical predictors of malignant pigmented lesions. A comparison of the Glasgow seven-point checklist and the American Cancer Society's ABCDs of pigmented lesions, " J Dermatol Surg Oncol 18(1), 22-26 (1992).

[5] Thomas, L, Tranchand, P., Berard, F., Secchi, T., Colin, C., Moulin, G., "Semiological value of ABCDE criteria in the diagnosis of cutaneous pigmented tumors," Dermatology 197(1), 11-17(1998).

[6] Jones, T.P., Boiko, P.E., Piepkorn, M.W., "Skin biopsy indications in primary care practice: a population-based study," J Am Board Farm Pract 9(6), 397-404 (1996).

[7] Bafounta, M.L., Beauchet, A., Aegerter, P., Saiag, P., "Is dermoscopy (epiluminescence microscopy) useful for the diagnosis of melanoma? Results of a meta-analysis using techniques adapted to the evaluation of diagnostic test," Arch Dermatol 137(10), 1343-50 (2001).

[8] Massone, C., Di Stefani, A., Soyer, H.P., "Dermoscopy for skin cancer detection," Curr Opin Oncol, 17(2), 147-153 (2005).

[9] Moncrieff, M., Cotton, S., Claridge, E., Hall, P., "Spectrophotometric intracutaneous analysis: a new technique for imaging pigmented skin lesions, " Br J Dermatol 146(3), 448-57 (2002).

[10] Terstappen, K., Suurkula, M., Hallberg, H., Ericson, M.B., Wennberg, A.M., "Poor correlation between spectrophotometric intracutaneous analysis and histopathology in melanoma and nonmelanoma lesions, " J Biomed Opt 18(6), 061223-061223 (2013).

[11] Gutkowicz-Krusin, D., Elbaum, M., Jacobs, A., Keem, S., Kopf, A.W., Kamino, H., Wang, S., Rubin, P., Rabinovitz, H., Oliviero, M., "Precision of automatic measurements of pigmented skin lesion parameters with a MelaFind multispectral digital dermoscope," Melanoma Res 10(6), 563-70 (2000).

[12] Lui, H., Zhao, J., McLean, D., Zeng, H., "Real-time Raman spectroscopy for in vivo skin cancer diagnosis," Cancer Res 72(10), 2491-500 (2012).

[13] Elbaum, M., Kopf, A.W., Rabinovitz, H.S., Langley, R.G., Kamino, H., Mihm, M.C.Jr., Sober, A.J., Peck, G.L., Bogdan, A., Gutkowicz-Krusin, D., Greenebaum, M., Keem, S., Oliviero, M., Wang, S., "Automatic differentiation of melanoma from melanocytic nevi with multispectral digital dermoscopy: a feasibility study," J Am Acad Dermatol, 44(2), 207-18 (2001).

[14] Bergstrom, K.G. (2012). MelaFind was approved by FDA: where does it fit in dermatology? *J Drugs Dermatol, 11*(3), 420-422.

[15] Zhao, J., Lui, H., McLean, D.I., Zeng, H. (2008). Real-time Raman spectroscopy for non-invasive skin cancer detection – preliminary results. Conf Proc IEEE Eng Med Biol Soc, 2008, 3107-9

[16] MacKinnon, N., Vasefi, F., Gussakovsky, E., Bearman, G., Chave, R., and Farkas, D.L., "In vivo skin chromophore mapping using a multimode imaging dermoscope (SkinSpect)", Proc. SPIE, 8587, 85870U (2013).

[17] Vasefi, F., MacKinnon, N. B., Farkas, D. L., "Toward in-vivo diagnosis of skin cancer using multimode imaging dermoscopy: (II) molecular mapping of highly pigmented lesions, , Proc. SPIE (In Press), 8947-18 (2014)

[18] Samatham, R., Lee, K., Jacques, S.L., "Clinical study of imaging skin cancer margins using polarized light imaging," Proc. SPIE 8207, 82070O (2012).

[19] Yuan, Y., "Investigation of skin and skin components using polarized fluorescence and polarized reflectance towards the detection of cutaneous melanoma," [dissertation]. Toledo (OH): University of Toledo (2006).

[20] Huang, Z., Cheah, H.M., Chia, T.C., Ching, T.L. (2000). Laser-induced microscopic fluorescence and images of skin tissues. *Proc. SPIE, 4164*, 43-47. Retrieved from http://adsabs.harvard.edu/abs/2000SPIE.4164...43H

[21] Sinichkin, Y.P., Utz, S.R., Mavliutov, A.H., Pilipenko, H.A. (1998). In vivo fluorescence spectroscopy of the human skin: experiments and models. *J Biomed Opt, 3*(2), 201-211.

[22] Yuanfang, L., Cameron, B.D., Relue, P.A. (2007). Fluorescence anisotropy of cellular NADH as a tool to study different metabolic properties of human melanocytes and melanoma cells. *IEEE J Sel Top Quantum Electron, 13*(6), 1671-1679.

[23] Yuan, Y., Relue, P. (2008). Enzymatic degradation of human skin dermis revealed by fluorescence and reflectance spectroscopy. *Opt. Express* 16, 9857-9868.

[24] Biswal, N., Gupta, S., Ghosh, N., Pradhan, A. (2003). Recovery of turbidity free fluorescence from measured fluorescence: an experimental approach. *Opt Express, 11*(24), 3320-31.

[25] Bradley, R. S., Thorniley, M. S. (2006). A review of attenuation correction techniques for tissue fluorescence. J R Soc Interface, 3(6), 1-13.